Int. J. Electrochem. Sci., 14 **(2019)** 9850 – 9857, doi: 10.20964/2019.10.47

International Journal of
ELECTROCHEMICAL
SCIENCE
www.electrochemsci.org

Short Communication

High-wettability and Fire Resistant Separator Efficient Polysulfide Barrier for Increased Electrochemical Activity

Jiaofei Huo[1,*], *Yinwei Wang*[2]

[1] Department of Mechanical and Electrical Technology, Xijing University, Xi'an 710123, China
[2] Intelligent Manufacturing Research and Development Center, Xijing University, Xi'an 710123, China
[*]E-mail: yinweiwangxj@yeah.net

Received: 31 May 2019 / *Accepted:* 26 June 2019 / *Published:* 30 August 2019

The common polypropylene separator could provide pathways for the transportation for the lithium-ions. However, it fails to inhibit the polysulfide migration during the electrochemical reactions. As a result, the functional separators must be developed for inhibiting the shuttle effect of the soluble polysulfide. In our work, nano fibrous separator is prepared and used as the efficient barrier for the polysulfide migration. The PSA separator is fabricated by electrospinning method, using polysulfonamide membrane as the functional separator in the lithium-sulfur batteries. The electrochemical result shows that the initial specific capacity of the PSA separator is as high as 1506 mAh g^{-1} at the current density of 0.05 C. The PSA separator shows capacity of 1052 mAh g^{-1} after 100 cycles at the current density of 0.2 C.

Keywords: Polysulfonamide, Shuttle Effect, Fire Retardant, Separator, Li-S Battery, Electrochemical Performance

1. INTRODUCTION

To satisfy the demand for the clean energy with the development of the science and technology, new rechargeable batteries are urgently demanded for the high specific capacity and high energy density [1, 2, 3]. Among current various energy storage systems, lithium-sulfur batteries are the most promising candidates for the next generation storage batteries due to their high specific capacity (1675 mAh g^{-1}) and high energy density (2600 Wh Kg^{-1}) [4, 5, 6]. Besides, the sulfur is natural abundance and non-toxicity [7, 8]. Nevertheless, there are also many disadvantages for the lithium-sulfur batteries [9]. Especially, the migration of the polysulfide delays the application of the lithium-sulfur batteries [10].

During the past decades, many works have been reported about the developments of the lithium-sulfur batteries [11]. To inhibit the shuttle effect of the polysulfide, various methods are applied for solving this problem, such as designing suitable host materials for the element sulfur, employing superior interlayers between the cathode and the separator, developing new type electrolyte for the lithium-sulfur batteries [12-15]. However, there are few studies about the employment of the functional separators in the lithium-sulfur batteries, which could efficiently adsorb the soluble polysulfide and inhibit its migration [16, 17]. Evidently, it is urgent to exploit new functional separators for restraining the migration of the polysulfide [18]. Yao et al used TiO_2@C nanofibers as efficient interlayer for high-performance lithium-sulfur battery [19]. Moreover, cobalt-embedded carbon nanofiber was applied as host materials for sulfur to catalysis the polysulfide redox reaction [20].

The traditional polypropylene separator is beneficial for the transportation of the lithium-ions. However, it fails to inhibit the polysulfide migration during the electrochemical reactions. Therefore, functional separators must be developed for inhibiting the shuttle effect of the soluble polysulfide. In this paper, nanofibrous separator is prepared and used as the barrier for the polysulfide migration. The PSA separator is fabricated by electrospinning method, using polysulfonamide membrane as the functional separator in the lithium-sulfur batteries.

2. EXPERIMENTAL SECTION

2.1. Preparation of PSA separator

1.2 g polysulfonamide was dispersed in 15 mL DMF under ultrasonication for 4 h. The electrospinning process was performed at a high voltage of 13 kV with a distance of 15 cm between the needle tip and collector, and a feeding rate of 0.5 ml h^{-1}. After that, the resultant separator was dried at 60 ℃ for 24 h to clear the solvent.

2.2. Materials Characterization

The morphologies of the samples were characterized by using scanning electron microscope (SEM, JSM-7100F). The contact angles were tested by using an automatic contact angle meter (Model SL200A/B/D).

2.3. Electrochemical Measurements

The electrochemical performance of the lithium-sulfur batteries was tested via using coin CR2032 half batteries. Firstly, the active materials, carbon black and PVDF were mixed with a ratio of 8:1:1 for preparing electrode slurry. Then, the slurry was uniformly coated on the surface of the Al film. After that, the film was transferred into vacuum under 80℃ for 24 h. The resultant film was used as the cathode. The as-prepared PSA separator and pristine separator were used as the separator in the

lithium-sulfur batteries, respectively. The lithium film was used as anode. The electrolyte was consisted of 1.0 M LiTFSI and DOL/DME (1:1). The constant discharge/charge profiles were carried out on a battery testing system (LandCT2001A) in the voltage between 1.5 V and 3 V.

3. RESULTS AND DISCUSSION

Figure 1a-c displays the morphologies of the PSA separator. As shown in Figure 1a, it can be seen that the surface of the PSA separator is smooth. Furthermore, it could be observed that the PSA separator shows nano fibrous structure on the surface. The dimeter of the fibers is located at 150-180 nm [21]. This nano fibrous structure provides channels for the transportation of the lithium-ions. Besides, it is beneficial for the wetting of the electrolyte in the lithium-sulfur batteries.

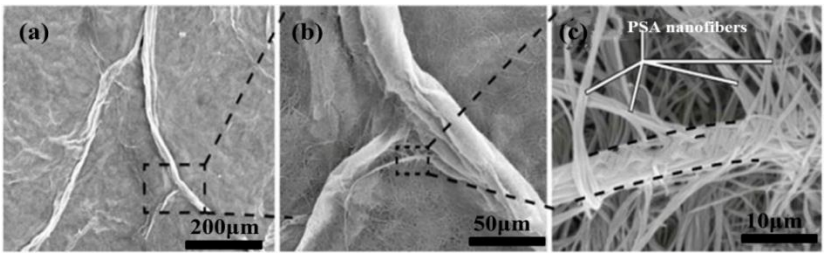

Figure 1. (a), (b) and (c) SEM images of the as-prepared PSA separator at different magnification.

Figure 2a shows the SEM image of the pristine Clegard 2300 separator. The pristine separator exhibits uniform porous structure. And the pore size of the pristine Clegard 2300 separator is about hundreds of nanometers. Figure 2b is the SEM iamge of the as-prepared PSA separator. It can be seen from the figure that the PSA separator displays nano fibrous morphology with porous structure. Comparing with the pristine separator, the PSA separator displays more abundant fibrous structure. Moreover, Figure 2c-e displays the wettability of the as-prepared PSA separator when immersed into the electrolyte. As shown in Figure 2c, the as-prepared PSA separator exhibits white membrane. During dipping into the electrolyte, the PSA separator displays excellent wettability (Figure 2d). After drying at the room temperature, the PSA separator could still keep its original shape, indicating excellent structure stability upon folding and immersing in the electrolyte.

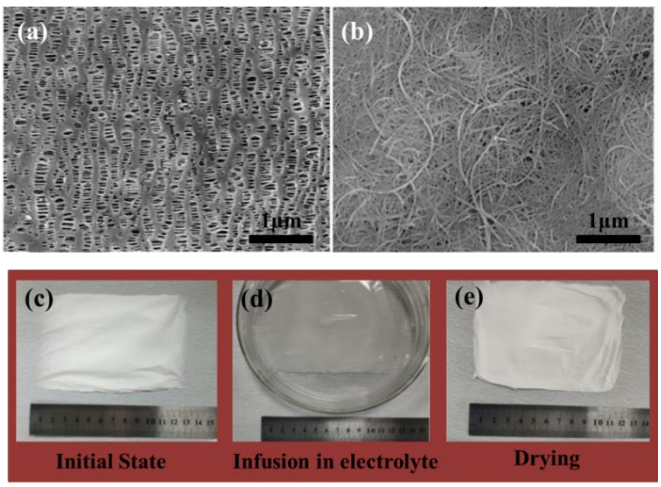

Figure 2. (a) SEM image of the pristine separator. (b) SEM image of the PSA separator. (c-e) Image for showing flexibility and high wettability of the PSA separator in the electrolyte.

Figure 3a and b shows the contact angles of the two kinds of separator. It can be seen that the contact angles are 45°and 28° in the electrolyte, respectively. This result further confirms more superior high-wettability of the PSA separator than pristine separator in the electrolyte [22]. The more superior high-wettability of PSA separator is beneficial for the transport of the Li^+ in the electrolyte between the cathode and anode. Figure 3 c shows the cross section SEM image of the PSA separator. It could be clearly observed that the PSA separator consist of many layers structure. This is consistent with the contact angle tests.

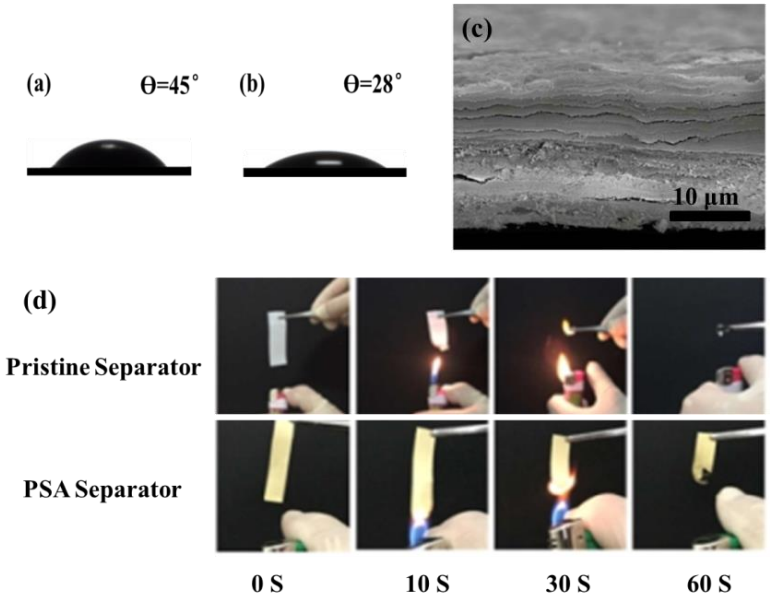

Figure 3. (a) and (b) contact angle tests for the pristine separator and PSA separator by using electrolyte. (c) Cross section SEM image of the PSA separator. (d) Images of flame test on pristine separator and PSA separator.

The layer structure could act as a vessel for the storage of the sufficient electrolyte. The safety of the batteries is one of the most important indexs for judging the electrochemical performance of the batteries. Therefore, fire test was conducted for the pristine separator and PSSA separator. As shown in Figure 3d, the pristine separator is easily ignited. After 60 s, the pristine separator becomes ashes. However, for the PSA separator, it is fire retardant. Consequently, the as-prepared PSA separator shows fire retardant ability, which is significant for the lithium-sulfur batteries.

Figure 4a shows the constant discharge/charge profiles of the pristine separator at various current densities from 0.05 C to 1 C. The lithium-sulfur battery by using pristine separator exhibits specific capacities of 1436 mAh g^{-1}, 1368 mAh g^{-1}, 1202 mAh g^{-1} and 936 mAh g^{-1} at the current densities of 0.05 C, 0.1 C, 0.2 C and 0.5 C, respectively [23, 24]. When the current density was improved to 1 C, the specific capacity is only 610 mAh g^{-1}. It can be seen that the specific capacities fade rapidly with the increase of the current densities. However, the lithium-sulfur battery by using PSA separator shows excellent electrochemical performance. The PSA separator displays initial specific capacities of 1506 mAh g^{-1}, 1398 mAh g^{-1}, 1265 mAh g^{-1} and 1000 mAh g^{-1} at the current densities of 0.05 C, 0.1 C, 0.2 C and 0.5 C, respectively. Even at the high current density of 1 C, the specific capacity of PSA separator is still at 812 mAh g^{-1}. This could confirm the PSA separator is beneficial for improving the initial specific capacity at various current densities.

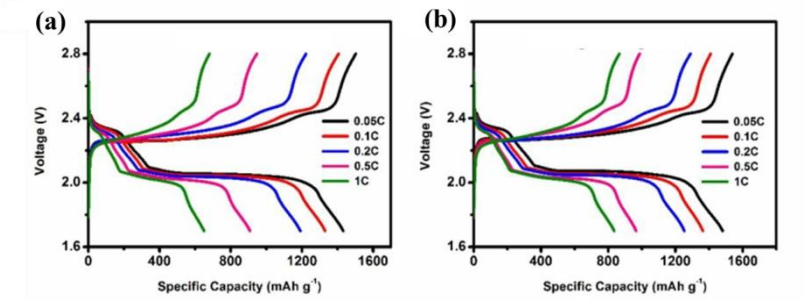

Figure 4. (a) and (b) The constant discharge/charge profiles of the Li-S battery by using pristine separator and PSA separator.

To investigate the chemical reaction in the lithium-sulfur batteries, CV tests were conducted for the pristine and PSA separator. As shown in Figure 5, the CV curves of the pristine separator and PSA separator exhibit same shape during the CV tests at various scanning rates. It can be seen that the area in the CV curves of the pristine separator becomes smaller with the increase of the scanning rates from 0.1 to 0.7 mV s^{-1}. This decrease is related to the migration of the polysulfide. As for the PSA separator, it shows typical and strong redox peaks at the scanning rate of 0.1 mV s^{-1}. Even at the high scanning rate of 0.7 mV s^{-1}, the CV curve of PSA separator still could keep well without obvious polarization.

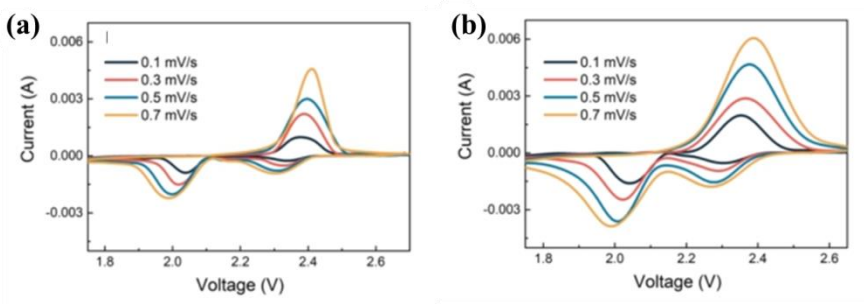

Figure 5. (a), (b) The CV profiles of the Li-S battery by using pristine separator and PSA separator, respectively.

To further verify the superior electrochemical performance of the PSA separator, rate capability is tested for the PSA separator at various current densities from 0.2 C to 3 C. As shown in Figure 6a, the PSA separator shows specific capacity of 1265 mAh g^{-1} at the current density of 0.2 C. When the current density is improved to 3 C, the specific capacity is as high as 501 mAh g^{-1}. Finally, the specific capacity value could recover back when the current density returns back to 0.2 C. Figure 6b shows the cycle performance of the PSA separator at the current density of 0.2 C for 100 cycles. It can be seen that the specific capacity of the PSA separator remains 1052 mAh g^{-1} after 100 cycles. This superior electrochemical performance is ascribed to the effect inhibition for the polysulfide.

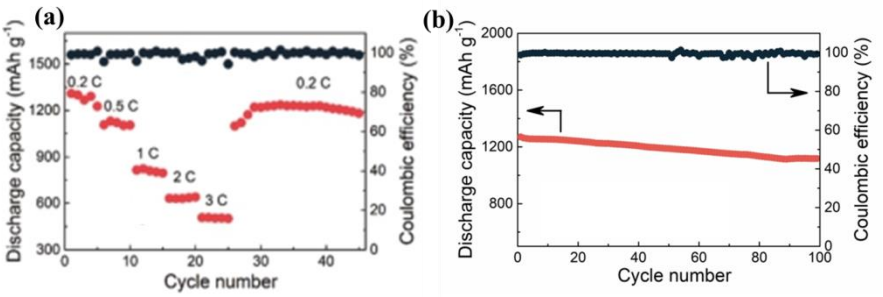

Figure 6. (a) Rate capability of the Li-S battery by using pristine separator and PSA separator. (b) Cycle performance of the Li-S battery that used pristine separator and PSA separator at the current density of 0.2 C for 100 cycles.

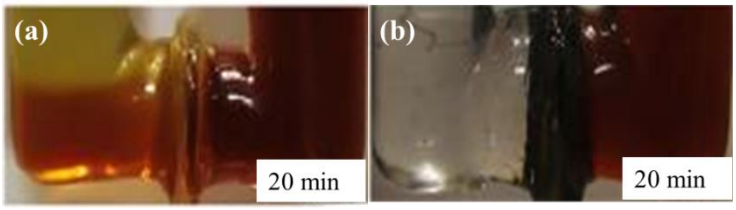

Figure 7. Polysulfide diffusion tests by using (a) pristine separator and (b) PSA separator.

Polysulfide adsorption tests were conducted, as shown in Figure 7. After 20 min, the color of the solution becomes brown in the both side of the device (Figure 7a). This phenomenon

demonstrates that the pristine separator fails to inhibit the shuttle effect of the polysulfide. While for the PSA separator, it can be clearly seen that the PSA separator could efficiently inhibit the migration of the soluble polysulfide.

4. CONCLUSIONS

In summary, nanofibrous PSA separator is prepared and used as the efficient barrier for the polysulfide migration. The separator is fabricated by electrospinning method, using polysulfonamide membrane as the functional separator in the lithium-sulfur batteries. The electrochemical result shows that the initial specific capacity of the PSA separator is as high as 1506 mAh g^{-1} at the current density of 0.05 C. The PSA separator shows capacity of 1052 mAh g^{-1} after 100 cycles at the current density of 0.2 C. This superior electrochemical performance is ascribed to the presence of the PSA separator, which could efficiently inhibit the polysulfide migration.

ACKNOWLEDGEMENT
This research is financially supported by the Xijing University.

References

1. Y. S. Lin, R. Pitcheri, J. G. Zhu, C. M. Jiao, Y. Guo, J. Li and Y. J. Qiu, *J. Alloy Compd*., 785 (2019) 627.
2. L. Wang, N. P. Deng, L. L. Fan, L. Y. Wang, G. Wang, W. M. Kang and B. W. Cheng, *Mater. Lett*., 233 (2018) 224.
3. Z. Wang, M. Feng, H. Sun, G. R. Li, Q. Fu, H. B. Li, J. Liu, L. Q. Sun, A. Mauger, C. M. Juilen, H. M. Xie and Z. W. Chen, *Nano Energ*., 59 (2019) 390.
4. M. D. Walle, K. Zeng, M. Y. Zhang, Y. J. Li and Y. N. Liu, *Appl. Surf. Sci*., 473 (2019) 540.
5. W. J. Qiu, C. H. An, Y. W. Yan, J. Xu, Z. J. Zhang, W. Guo, Z. Wang, Z. J. Zheng, Z. B. Wang, Q. B. Deng and J. S. Li, *J. Power Sources*, 423 (2019) 98.
6. Q. F. Peng, F. Yu, W. K. Wang, A. B. Wang, F. Wang and Y. Q. Huang, *Electrochim. Acta*, 299 (2019) 749.
7. Z. Li, L. B. Tang, X. H. Liu, T. B. Song, Q. J. Xu, H. M. Liu and Y. G. Wang, *Electrochim. Acta*, 310 (2019) 1.
8. Z. P. Ma, F. Y. Jing, Y. Q. Fan, J. J. Li, Y. Zhao and G. J. Shao, *J. Alloy Compd*., 789 (2019) 71.
9. L. X. Yin, G. Y. Xu, P. Nie, H. Dou and X. G. Zhang, *Chem. Eng. J*., 352 (2018) 695.
10. Y. D. Li, Q. Wang, D. G. Zheng, W. P. Li and J. X. Wang, *J. Alloy Compd*., 787 (2019) 982.
11. Z.X . Guang, Y. Huang, X. F. Chen, X. Sun, M. Y. Wang, X. S. Feng, C. Chen and X. D. Liu, *Electrochim. Acta*, 307 (2019) 260.
12. X. Y. Qian, D. Zhao, L. N. Lin, X. Q. Shen, S. S. Yao, D. W. Rao, Y. Y. Zhou and X. M. Xi, *Mater. Res. Bull*., 94 (2017) 104.
13. Z. Y. Zhang, Y. Q. Lai, Z. A. Zhang, K. Zhang and J. Li, *Electrochim. Acta*, 129 (2014) 55.
14. S. P. Li, Z. L. Han, W. Hu, L. F. Peng, J. Q. Yang, L. H. Wang, Y. Y. Zhang, B. Shan and J. Xie, *Nano Energ*., 60 (2019) 153.
15. P. Zeng, L. W. Huang, X. L. Zhang, Y. M. Han and Y. G. Chen, *Appl. Surf. Sci*., 427 (2018) 242.
16. B. Y. Hao, H. Li, W. Lv, Y. B. Zhang, S. Z. Niu, Q. Qi, S. J. Xiao, J. Li, F. Y. Kang and Q. H. Yang, *Nano Energ*., 60 (2019) 305.

17. D. H. Lee, J. H. Ahn, M. S. Park, A. Eftekhari and D. W. Kim, *Electrochim. Acta*, 283 (2018) 1291.
18. Z. Y. Zhang, Y. Q. Lai, Z. A. Zhang and J. Li, *Solid State Ionics*, 278 (2015) 166.
19. S. S. Yao, H. Tang, M. Q. Liu, L. L. Chen, M. X. Jing, X. Q. Shen and J. L. Tan, *J. Alloy Compd*., 788 (2019) 639.
20. S. P. Li, X. Chen, F. Hu, R. Zeng, Y. H. Huang, L. X. Yuan and J. Xie, *Electrochim. Acta*, 304 (2019) 11.
21. Q. S. Wang, Z. Y. Wen, J. H. Yang, J. Jin, X. Huang, X. W. Wu and J.D. Han, *J. Power Sources*, 306 (2016) 347.
22. W. Yang, W. Yang, J. N. Feng, Z. P. Ma and G. J. Shao, *Electrochim. Acta*, 210 (2016) 71.
23. Z. C. Song, X. L. Lu, Q. Hu, J. Ren, W. Q. Zhang, Q. J. Zheng and D. M. Lin, *J. Power Sources*, 421 (2019) 23.
24. H. Pan, X. X. Huang, R. Zhang, D. Wang, Y. T. Chen, X. M. Duan and G. W. Wen, *Chem. Eng. J*., 358 (2019) 1253.